Wave-vector-dependent spin filtering and spin transport through magnetic barriers in graphene

L. Dell'Anna[1] and A. De Martino[2]

[1]*International School for Advanced Studies (SISSA), Via Beirut 2-4, I-34014 Trieste, Italy*
[2]*Institut für Theoretische Physik, Universität zu Köln, Zülpicher Straße 77, D-50937 Köln, Germany*

We study the spin-resolved transport through magnetic nanostructures in monolayer and bilayer graphene. We take into account both the orbital effect of the inhomogeneous perpendicular magnetic field as well as the in-plane spin splitting due to the Zeeman interaction and to the exchange coupling possibly induced by the proximity of a ferromagnetic insulator. We find that a single barrier exhibits a wave-vector-dependent spin filtering effect at energies close to the transmission threshold. This effect is significantly enhanced in a resonant double barrier configuration, where the spin polarization of the outgoing current can be increased up to 100% by increasing the distance between the barriers.

I. INTRODUCTION

The electronic properties of graphene[1,2] have attracted in the last four years huge experimental as well as theoretical attention.[3] Besides its fundamental interest as a new type of two-dimensional electron liquid, graphene is, in fact, regarded as a promising material for future nanoelectronic devices,[3] in particular, in the field of spintronics,[4] due to its small intrinsic spin-orbit[5–7] and hyperfine interactions.[8] Indeed several recent experiments[9–12] have by now demonstrated spin injection and detection in a single layer of graphene sandwiched between ferromagnetic metal electrodes and observed coherent spin transport over micrometer scale distances.

Motivated by these developments, in this paper we focus on the problem of spin-resolved transport through *magnetic nanostructures* in graphene. The studies of graphene's transport properties through magnetic barriers and more complex structures[13–29] address the problem of controlling the confinement and the transport of charge carriers by means of appropriate configurations of an external magnetic field inhomogeneous on submicron scales. Different types of magnetic nanostructures have been envisioned and their properties investigated, e.g., barriers,[13,20–22] dots,[13] wires,[16] and superlattices.[25–29]

In all these works the spin degree of freedom has been completely neglected. This is justified because of the smallness of both Zeeman splitting and spin-orbit coupling (SOC) in graphene.[5–7] However, the continuous and rapid improvements in sample preparation and experimental technology and resolution in graphene research call for a refinement of the theoretical analysis to incorporate such finer effects. More importantly, it has recently been argued that local ferromagnetic correlations can be induced in graphene by several different mechanisms, e.g., proximity of a ferromagnetic insulator,[30–32] Coulomb interactions,[33] presence of defects,[34] and application of an electric field in the transverse direction in nanoribbons.[35] The ferromagnetism leads to a spin splitting effectively similar to a Zeeman interaction but of much larger magnitude. For example, a ferromagnetic insulator deposited on top of a graphene layer has been predicted to produce a spin splitting of up to 5 meV.[30] This is comparable

with the orbital energy in a field of 1 T, which is on the order of 25 meV, and thus may have important effects. The spin transport through ferromagnetic graphene has already received some attention,[30,31,36–39] but all works so far have focused only on spin effects and did not consider orbital effects. The aim of this paper then is to fill the gap and investigate this problem by fully taking into account the quasiparticle's spin dynamics as well as its orbital motion in an inhomogeneous magnetic field.

In this paper we shall focus on the effects of Zeeman and exchange spin splitting and postpone the interesting problem of spin-orbit coupling to a future work. We show that the spin-resolved transmissions exhibit a strong dependence on the incidence angle, which allows, in principle, for a selective transmission of spin-up and spin-down electrons. This effect can be qualitatively understood by a simple semiclassical argument. The bending of the electron trajectories under the barrier depends on the energy and thus, in the presence of spin splitting, is different for the two spin projections. The magnitude of the polarization that can be achieved depends on the spin splitting and can be very large in the presence of a large splitting, as, e.g., that originating from a proximity-induced exchange field. Moreover, in a resonant double barrier configuration, the polarization can be enhanced by increasing the distance between the barriers. In this case, in fact, even for relatively small splitting there exists an energy range where the polarization reaches values close to one for large enough distance.

While there exist several experimental techniques to produce magnetic barriers, for concreteness we shall have in mind the case of the fringe fields created by a ferromagnetic stripe deposited on top of the graphene sample. The magnetic field generated by the stripe is known analytically.[40] The corresponding vector potential in the Landau gauge can be written as $\mathbf{A} = A(x,z)\hat{y}$, where

$$A(x,z) = \left[\int_{-\infty}^{x} B_z(x',0)dx' - \int_{0}^{z} B_x(x,z')dz' \right], \quad (1)$$

and we assume that the system is translationally invariant in the y direction. We shall neglect possible corrugations of graphene and assume that it lies flat in the $z=0$ plane. Then

the orbital dynamics is only affected by the perpendicular component B_z, while both B_x and B_z contribute to the Zeeman interaction. In addition we shall also include in the Zeeman term the effects of a possible exchange field.[30,31]

The transport properties of such structures can be calculated by means of the Landauer-Büttiker formalism in terms of the spin-resolved transmission matrix $t_{\sigma\sigma'}$, which gives the probability amplitude for a quasiparticle incident on the magnetic structure from the left with spin projection σ' to be transmitted with spin σ.[41–44] The matrix $t_{\sigma\sigma'}$ depends on particle's energy E and incidence angle ϕ (see below) and must satisfy certain general symmetry requirements.[41] We shall be interested in the spin-resolved conductances

$$G_{\sigma\sigma'} = G_0 \int_{-\pi/2}^{\pi/2} d\phi \, \cos \phi |t_{\sigma\sigma'}|^2, \qquad (2)$$

and, with total conductance $G = \sum_{\sigma\sigma'} G_{\sigma\sigma'}$ and spin-quantization axis along the x direction, in the polarization vector of transmitted current for a spin-unpolarized incident current[43]

$$\mathcal{P}_x = \frac{G_0}{G} \sum_{\sigma\sigma'} \sigma |t_{\sigma\sigma'}|^2, \qquad (3)$$

$$\mathcal{P}_y = \frac{2G_0}{G} \Re \sum_{\sigma} t_{\uparrow\sigma} t_{\downarrow\sigma}^*, \qquad (4)$$

$$\mathcal{P}_z = \frac{2G_0}{G} \Im \sum_{\sigma} t_{\uparrow\sigma}^* t_{\downarrow\sigma}, \qquad (5)$$

with $G_0 = \frac{2e^2}{h} \frac{EL_y}{2\pi\hbar v_F}$ and in their integrated value

$$P_i = \int_{-\pi/2}^{\pi/2} d\phi \, \cos \phi \mathcal{P}_i. \qquad (6)$$

The rest of this paper is organized as follows. In Sec. II we discuss the spin-dependent transmission and transport through rectangular and double resonant barriers in single-layer graphene. In Sec. III we address the same problem in bilayer graphene and finally in Sec. IV we draw our conclusions.

II. SINGLE-LAYER GRAPHENE

Let us then start focusing on single-layer graphene. We shall neglect disorder and interaction effects and focus on a single K point, where ballistic motion of charge carriers in an external magnetic field $\mathbf{B} = B_x\hat{x} + B_z\hat{z}$, is described by the Dirac-Weyl (DW) Hamiltonian

$$H = v_F \boldsymbol{\tau} \cdot \left(\mathbf{p} + \frac{e}{c}\mathbf{A} \right) + H_{spin}, \qquad (7)$$

$$H_{spin} = \frac{g_s \mu_B}{2} \mathbf{B}^{eff} \cdot \boldsymbol{\sigma}, \qquad (8)$$

where $\mathbf{p} = p_x\hat{x} + p_y\hat{y}$, $v_F \approx 10^6$ m/s is the Fermi velocity, μ_B is the Bohr magneton and $g_s \approx 2$ is the effective Landé factor.
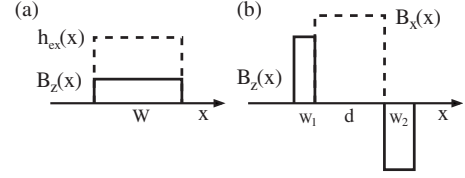

FIG. 1. Profiles of magnetic field and exchange field considered in this paper. In case (b) the exchange field is included in B_x.

H_{spin} is the sum of the Zeeman interaction due to the magnetic field and, possibly, the proximity-induced exchange splitting, with an estimated value[30] $h_{ex} \approx 5$ meV (corresponding to a Zeeman interaction with a field of about 86 T). The vector of Pauli matrices $\boldsymbol{\tau} = \tau_x\hat{x} + \tau_y\hat{y}$ (resp. $\boldsymbol{\sigma} = \sigma_x\hat{x} + \sigma_y\hat{y} + \sigma_z\hat{z}$) acts in sublattice space (resp. spin space), and the wave function Ψ is a four-component object, $\Psi^T = (\Psi_{A\uparrow}, \Psi_{B\uparrow}, \Psi_{A\downarrow}, \Psi_{B\downarrow})$ (the superscript T denotes transposition). $\mathbf{A} = A(x,z)\hat{y}$ is the vector potential in the Landau gauge, with $A(x,z)$ given in Eq. (1). Since the Hamiltonian is translationally invariant in the y direction and p_y is conserved, the wave function can be written as $\Psi = e^{ik_y y}\psi$ and the DW equation reduces to a one-dimensional problem. In the following we use rescaled quantities: $x \to x\ell_B$, $k_{x,y} \to k_{x,y}\ell_B^{-1}$, $A \to AB\ell_B$, and $E \to E\frac{\hbar v_F}{\ell_B}$, where B is a typical value of magnetic field in the problem. The magnetic length is $\ell_B = (\frac{\hbar c}{eB})^{1/2} \approx 26/\sqrt{B[\text{T}]}$ nm and the orbital energy scale is $E_m = \frac{\hbar v_F}{\ell_B} \approx 25\sqrt{B[\text{T}]}$ meV, where $B[\text{T}]$ is the magnetic field strength expressed in Tesla.

A. Rectangular barrier

First we discuss the tunneling of a spinful DW quasiparticle through a rectangular magnetic barrier of width W with an effective Zeeman field

$$\mathbf{B}^{eff} = \lambda \theta(W/2 - |x|)\hat{z}, \qquad (9)$$

see Fig. 1(a). The value of λ ranges from 0.002 for a Zeeman field of 1 T up to $\lambda \approx 0.2$ if an exchange splitting of 5 meV is included. With spin-quantization axis along $\hat{z}$, Hamiltonian (7) is diagonal in spin space and the two spin components can be treated separately. Accordingly, the wave function for fixed spin projection is a two-component (sublattice) spinor. The solution to Eq. (7) with energy E (assumed positive for definiteness) and spin projection σ describing a scattering state incoming from the left can be written in the left and right "leads" (i.e., the nonmagnetic regions $x < -W/2$ and $x > W/2$) as

$$\psi_\sigma(x < -W/2) = \frac{1}{\sqrt{k_x^i}} \mathcal{W}_0(x) \begin{pmatrix} 1 \\ r_{\sigma\sigma} \end{pmatrix}, \qquad (10)$$

$$\psi_\sigma(x > W/2) = \frac{1}{\sqrt{k_x^f}} \mathcal{W}_0(x) \begin{pmatrix} t_{\sigma\sigma} \\ 0 \end{pmatrix}, \qquad (11)$$

where $r_{\sigma\sigma'}$ (resp. $t_{\sigma\sigma'}$) is the probability amplitude for a quasiparticle incident from the left with spin projection σ' to be reflected (resp. transmitted) with spin σ. The matrix $\mathcal{W}_0$ is given by

$$\mathcal{W}_0(x) = \begin{pmatrix} 1 & 1 \\ e^{i\phi(x)} & -e^{-i\phi(x)} \end{pmatrix} e^{i\tau_z k_x(x)x} \qquad (12)$$

with $k_x(x) = \sqrt{E^2 - [k_y + A(x)]^2}$ and $\pm e^{\pm i\phi(x)} = \frac{\pm k_x(x) + i[k_y + A(x)]}{E}$. In the leads we use the parameterization:

$$k_y = E \sin \phi_i = E \sin \phi_f - \Phi, \qquad (13)$$

$$k_x^i = k_x(x < -W/2) = E \cos \phi_i, \qquad (14)$$

$$k_x^f = k_x(x > W/2) = E \cos \phi_f, \qquad (15)$$

where $\Phi = A(x > W/2)$ is the total perpendicular magnetic flux through the barrier per unit length in the y direction. For $\Phi > 0$ the emergence angle ϕ_f is larger than the incidence angle ϕ_i. Thus a finite transmission is only possible if ϕ_i is smaller than the critical angle $\phi_c = \arcsin(1 - \Phi/E)$. For energy smaller than the threshold value $E_{th} = |\Phi|/2$ the transmission vanishes for any incidence angle.[13,25] This condition has a simple geometrical interpretation. In momentum space the dispersion cone after the barrier is shifted with respect to the cone in the region before the barrier by $-\Phi$ along the k_y axis. Thus if the radius of the fixed energy circle (the Fermi line) is smaller than $\Phi/2$, the equal energy sections of the two cones do not overlap, implying that k_x^f is imaginary for any k_y, i.e., the barrier is perfectly reflecting. Note that neither the emergence angle ϕ_f nor the critical angle ϕ_c depends on spin. In the barrier region $|x| < W/2$ the spin-σ wave function can be written as[13]

$$\psi_\sigma(x) = \mathcal{W}_B^\sigma(x) \begin{pmatrix} a \\ b \end{pmatrix}, \qquad (16)$$

$$\mathcal{W}_B^\sigma(x) = \begin{pmatrix} D_{p_\sigma}(q) & D_{p_\sigma}(-q) \\ \dfrac{i\sqrt{2}}{E_\sigma} D_{p_\sigma+1}(q) & \dfrac{-i\sqrt{2}}{E_\sigma} D_{p_\sigma+1}(-q) \end{pmatrix}, \qquad (17)$$

where $D_p(z)$ is the parabolic cylinder function,[45] $q = \sqrt{2}[A(x) + k_y]$, $p_\sigma = \frac{E_\sigma^2}{2} - 1$, $E_\sigma = E - \sigma\lambda$, and a and b complex amplitudes. Continuity of the wave function then leads to the matching condition across the magnetic barrier

$$\begin{pmatrix} 1 \\ r_{\sigma\sigma} \end{pmatrix} = \left(\frac{\cos \phi_i}{\cos \phi_f} \right)^{1/2} \hat{T} \begin{pmatrix} t_{\sigma\sigma} \\ 0 \end{pmatrix}, \qquad (18)$$

where the (spin-dependent) transfer matrix $\hat{T}$ is given by

$$\hat{T} = [\mathcal{W}_0(-W/2)]^{-1} \mathcal{W}_B^\sigma(-W/2) [\mathcal{W}_B^\sigma(W/2)]^{-1} \mathcal{W}_0(W/2).$$

The transmission coefficient can directly be read from Eq. (18)

$$|t_{\sigma\sigma}|^2 = \frac{\cos \phi_f}{\cos \phi_i} \frac{1}{|T_{11}|^2}. \qquad (19)$$

The spin-resolved transmission as a function of the incidence angle is illustrated in Fig. 2 for two different barrier widths. Remarkably we find that, even though the critical angle ϕ_c is the same for both spin projections, there is a large difference between the spin-up and spin-down transmissions
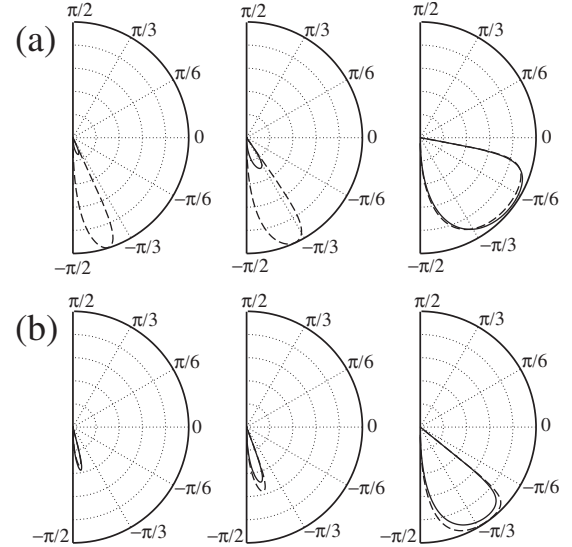

FIG. 2. (a) Angular plot of the transmission (as a function of the incidence angle ϕ_i) through a rectangular magnetic barrier of width $W = 2$ (in units of ℓ_B) with $\lambda = 0.2$ for spin-up (solid lines) and spin-down (dashed lines) quasiparticles at energy $E = 1.05$, 1.1, and 1.7 (from left to right, in units of E_m); (b) the same for a barrier of width $W = 6$ at energy $E = 3.05$, 3.1, and 3.7. Here we set $B = 1$ T, so that $E_m \approx 25$ meV and an energy increment of 0.1 corresponds to 2.5 meV.

within an energy range λ from the common threshold energy E_{th}, see Fig. 2(a). This is due to the very sharp angular and energy dependences of the transmission onset. However, this effect becomes very small as soon as $\lambda/E_{th} \ll 1$, as one can see in Fig. 2(b), where $E_{th} = 3$.

Before moving to more complex structures, it is interesting to briefly consider the limit $B \to \infty$, $W \to 0$ with fixed $BW = \Phi$, where the magnetic field profile reduces to a δ function, $B(x) = \Phi\delta(x)$. Using the asymptotic behavior of the parabolic cylinder function $D_p(z)$ for $p \to \infty$ and $z \to 0$ with $z\sqrt{p}$ finite[46]

$$D_{-p-1}(\pm iz) = \frac{\sqrt{\pi}(p/e)^{p/2}}{\Gamma(1+p)} e^{\mp iz\sqrt{p}} [1 + O(p^{-1/2})],$$

after some lengthy algebra we obtain the compact result

$$\mathcal{W}_B^\sigma(-W/2)[\mathcal{W}_B^\sigma(W/2)]^{-1} \to e^{i\sigma\lambda_z\tau_x}, \qquad (20)$$

where the dimensionless Zeeman coupling is now given by $\lambda_z = \frac{\mu_B\Phi}{\hbar v_F}$. An elementary calculation then obtains the transmission as

$$|t_{\sigma\sigma}|^2 = \frac{\cos \phi_i \cos \phi_f}{\cos^2 \lambda_z \cos^2 \dfrac{\phi_i + \phi_f}{2} + \sin^2 \lambda_z \cos^2 \dfrac{\phi_i - \phi_f}{2}}, \qquad (21)$$

which, in contrast to the case of a barrier of finite width, is spin independent. We note that if one solves the scattering problem by considering Hamiltonian (7) directly with $\mathbf{B}^{eff} = BW\delta(x)\hat{z}$ and imposing the matching condition obtained by integrating Eq. (7) across the origin with the prescription $\delta(x)\theta(x) = \delta(x)/2$, one obtains Eq. (21) with λ_z replaced by
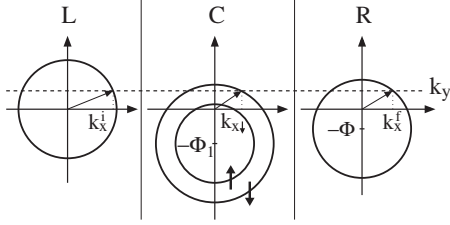
FIG. 3. Illustration of the kinematics of the transmission through a resonant double magnetic barrier. The solid circles represent the constant-energy contours (Fermi lines) in the region before (resp. after) the structure (L, resp. R) or in between the barriers (C). In the leads L and R the circles are doubly spin degenerate. In C the vector potential shifts the cones along the k_y axis, so they are centered at $k_x=0$, $k_y=-\Phi_1$. The spin splitting in C shifts the cones upwards (resp. downwards) for spin up (resp. spin down), such that the Fermi line shrinks (resp. widen). The horizontal dashed line represents the fixed y component of the momentum, conserved across the barriers. $\Phi=\Phi_1+\Phi_2$ is the total flux through the structure (per unit length in the y direction). It is clear from the picture that if $|E-\lambda_x|<|k_y+\Phi|<|E+\lambda_x|$ a spin-up particle propagates in C via an evanescent wave.

$\widetilde{\lambda}_z=2\arctan\frac{\lambda_z}{2}$. The precise functional dependence of the transmission on the δ-function strength depends, in fact, on the regularization, similarly to the case of an electrostatic barrier.[47] Since the use of the prescription $\delta(x)\theta(x)=\delta(x)/2$ in the DW first-order differential equation has been criticized,[47] in the rest of the paper we shall use Eq. (20).

B. Resonant double barrier

We now discuss the case of a resonant structure consisting of two rectangular magnetic barriers with opposite signs of the magnetic field and nonvanishing in-plane Zeeman splitting in between, as illustrated in Fig. 1(b)

$$\mathbf{B}=\begin{cases}B\hat{z}, & 0<x<W_1\\ B_x\hat{x}, & W_1<x<W_1+d\\ -B\hat{z}, & W_1<x-d<W_1+W_2\\ 0, & \text{otherwise}.\end{cases} \quad (22)$$

This profile should qualitatively model the realistic configuration of the stray field produced by a ferromagnetic stripe, which, in addition to the normal component, also contains an in-plane component B_x. Inclusion of this component is crucial for the proper treatment of the spin dynamics.[42]

First, we neglect the Zeeman term under the barriers, so that the problem is again diagonal in spin, with spin-quantization axis along the x direction. By way of a simple geometric argument, illustrated in Fig. 3, we argue that this structure exhibits a strong wave-vector-dependent spin-filtering effect. Indeed, in the region C between the barriers the dispersion cones for spin-up and spin-down particles are equally shifted by $-\Phi_1=-BW_1$ along the k_y axis with respect to the cones in the left (L) lead. Moreover the cones are also shifted (say for $B_x>0$) upward (resp. downward) by the in-plane Zeeman splitting, so that the radius (the Fermi momentum) increases (resp. decreases) by $\lambda_x=\mu_B B_x/E_m$. As a result
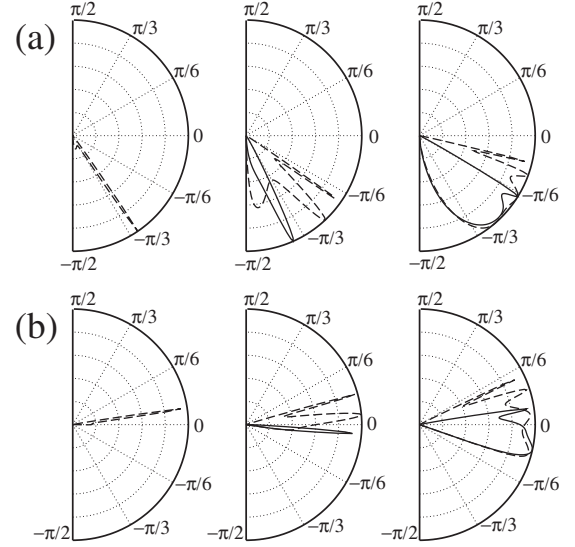

FIG. 4. Angular plot of the transmission (as a function of the incidence angle ϕ_i) for the profile in Fig. 1(b) with $d=6$, $\lambda_x=0.2$, and $\lambda_z=0$. Solid lines are for spin up and dashed lines for spin down. (a) Barriers of equal width $W_1=W_2=2$ (in units of ℓ_B) and energy $E=1.02$, 1.18, and 1.5 (from left to right, in units of E_m); (b) the same as in (a) but for barriers of different widths ($W_1=1$ and $W_2=2$).

there exists a range of incidence angles in which the spin-down modes propagate via traveling waves in the central region, whereas the spin-up modes only exist as evanescent waves and their transmission through the structure is exponentially suppressed with the distance between the barriers. Formally, this can easily be seen from the expression of the x component of the momentum in the region C, $k_{x\sigma}=\sqrt{(E-\sigma\lambda_x)^2-(k_y+\Phi_1)^2}$, which is real for $\sigma=\downarrow=-$ and pure imaginary for $\sigma=\uparrow=+$ as long as $|E-\lambda_x|<|k_y+\Phi|<|E+\lambda_x|$. If $|E-\lambda_x|>\Phi/2$ the transmission $|t_{\uparrow\uparrow}|^2$ at any incidence angle is fully suppressed for large enough d and spin-up modes do not significantly contribute to the transport through the structure.

We note in passing that a similar kinematic argument, with few minor modifications, should also work in the case of a two-dimensional electron gas (2DEG). Indeed, spin filtering in transport through magnetic structures has also extensively been discussed in 2DEG with qualitatively similar results (see, e.g., Ref. 42, and references therein), though to the best of our knowledge not in terms of such a simple kinematic explanation.

The exact calculation of the transmission coefficients follows the same lines as for the single rectangular barrier discussed in the previous section. The results are illustrated in Fig. 4. Figure 4(a) shows indeed that in a certain range of incidence angles the transmission for spin-up particles practically vanishes. By changing the ratio of barrier widths W_1/W_2 one can also control the position of the center of this interval, as illustrated in Fig. 4(b). The width of this range clearly depends on λ_x. It is then crucial to have a large in-plane spin splitting if one is to observe this effect.

A simple closed formula for the transmission is easily obtained in the limit of δ barriers of equal and opposite strengths $\Phi_1=-\Phi_2=\Phi$

$$|t_{\sigma\sigma}|^2 = \frac{(\cos k_{x\sigma}d)^{-2}}{1 + \frac{[k_y(k_y+\Phi) - E(E-\sigma\lambda_x)]^2}{(k_x^i)^2 k_{x\sigma}^2}\tan^2 k_{x\sigma}d}, \quad (23)$$

which explicitly exhibits the features discussed above and qualitatively reproduces the transmission for the case of double rectangular barriers. Resonances occur at $k_{x\sigma}d = \pi n$, with n a positive integer, where $|t_{\sigma\sigma}|^2 = 1$. Upon increasing d, the number of resonances increases and they also become narrower. Interestingly, the positions of the resonances are different for spin-up and spin-down electrons.

Next we consider the general situation where we do not neglect the Zeeman splitting under the barriers. Then with spin-quantization axis along the x direction, spin flips can take place at the barriers, hence, in contrast to the previous case, an incident particle upon transmission or reflection can change its spin state and the spin-filtering effect be spoiled. As we will see, however, the effect still survives close to some thresholds.

In this case the wave function must be written as

$$\psi = \sum_{\sigma=\pm} \psi_\sigma|\sigma\rangle = \begin{pmatrix} \psi_\uparrow \\ \psi_\downarrow \end{pmatrix}, \quad (24)$$

where $|\sigma = \pm = \uparrow\downarrow\rangle$ are the eigenstates of σ_x with eigenvalue $\sigma = \pm 1$ and ψ_σ are two-component sublattice spinors. The solution to Eq. (7) with energy E for a state incoming from the left with spin projection σ can be written in the left and right leads as

$$\psi(x<0) = \frac{1}{\sqrt{k_x(x)}}\mathcal{W}(x)\begin{pmatrix} \delta_{\uparrow,\sigma} \\ r_{\uparrow\sigma} \\ \delta_{\downarrow,\sigma} \\ r_{\downarrow\sigma} \end{pmatrix}, \quad (25)$$

$$\psi(x>d) = \frac{1}{\sqrt{k_x(x)}}\mathcal{W}(x)\begin{pmatrix} t_{\uparrow\sigma} \\ 0 \\ t_{\downarrow\sigma} \\ 0 \end{pmatrix}, \quad (26)$$

where $\delta_{\sigma,\sigma'}$ is the Kronecker delta and we introduce the 4×4 matrix $\mathcal{W}$ given by

$$\mathcal{W}(x) = \begin{pmatrix} e^{ik_{x\uparrow}(x)x} & e^{-ik_{x\uparrow}(x)x} & 0 & 0 \\ e^{i\phi_\uparrow(x)}e^{ik_{x\uparrow}(x)x} & -e^{-i\phi_\uparrow(x)}e^{-ik_{x\uparrow}(x)x} & 0 & 0 \\ 0 & 0 & e^{ik_{x\downarrow}(x)x} & e^{-ik_{x\downarrow}(x)x} \\ 0 & 0 & e^{i\phi_\downarrow(x)}e^{ik_{x\downarrow}(x)x} & -e^{-i\phi_\downarrow(x)}e^{-ik_{x\downarrow}(x)x} \end{pmatrix}, \quad (27)$$

with

$$k_{x\sigma} = \sqrt{(E-\sigma\lambda_x)^2 - (k_y+A)^2} \quad (28)$$

$$\pm e^{\pm i\phi_\sigma} = \frac{\pm k_{x\sigma} + i(k_y+A)}{E-\sigma\lambda_x}. \quad (29)$$

The transfer matrix is then given by

$$\hat{T} = \mathcal{W}(0^-)^{-1}\Omega(+)\mathcal{W}(0^+)\mathcal{W}(d^-)^{-1}\Omega(-)\mathcal{W}(d^+),$$

where the 4×4 matrix $\Omega(\pm) = e^{\pm i\lambda_z\tau_x\sigma_z}$ (nondiagonal in spin space) implements the matching conditions at the δ barriers, and $x^\pm \equiv x \pm 0^+$. For an incident particle with spin σ the continuity condition implies

$$\begin{pmatrix} \delta_{\uparrow,\sigma} \\ r_{\uparrow\sigma} \\ \delta_{\downarrow,\sigma} \\ r_{\downarrow\sigma} \end{pmatrix} = \left(\frac{\cos\phi_i}{\cos\phi_f}\right)^{1/2}\hat{T}\begin{pmatrix} t_{\uparrow\sigma} \\ 0 \\ t_{\downarrow\sigma} \\ 0 \end{pmatrix}, \quad (30)$$

from which the transmission amplitudes $t_{\sigma\sigma'}$ are easily obtained. Then using Eqs. (2)–(5) we can calculate the spin-resolved conductance and the spin polarization of the outgoing current for an unpolarized incoming current. The results are illustrated in Figs. 5–8. The x component of the polariza-tion vector P_x is plotted in Fig. 5 as a function of energy for different values of the distance d between the two magnetic barriers. Just for convenience, here and below we take B_x^{eff} negative, so that the spin-up current is favored against the spin-down current and P_x is mostly positive. For the Zeeman couplings we use the values $\lambda_x = \mu_B B_x/E_m \approx -0.0025$ and $\lambda_z = \lambda_x\frac{B}{B_x}\frac{W}{\ell_B} \approx 0.005$ corresponding to $-B_x = B = 1$ T and $W = 2\ell_B \approx 50$ nm. The spin-resolved conductances $G_{\uparrow\uparrow}$ and $G_{\downarrow\downarrow}$ are plotted in the inset of Fig. 5. The conductance $G_{\downarrow\downarrow}$ is slightly lower than $G_{\uparrow\uparrow}$ while $G_{\uparrow\downarrow} = G_{\downarrow\uparrow}$ are negligibly small. There is then a very narrow energy region, close to $E = E_{th}$ ($E_{th} = 1$ for $B = 1$ T and $W = 2\ell_B$), in which $G_{\uparrow\uparrow}$ and $G_{\downarrow\downarrow}$ are different (see the inset in Fig. 5), and P_x exhibits a narrow peak. We checked that, with these values of the parameters, P_y and P_z are of order 10^{-3}–10^{-4}, thus negligible, and P_x gives the most important contribution to the total polariza-tion $|P| = \sqrt{P_x^2 + P_y^2 + P_z^2}$. We have calculated $|P|$ for different values of the distance between the barriers d and found that the polarization maximum increases with d. This behavior is clearly seen in Fig. 6, where the maximum of $|P|$ is plotted as a function of d. The energy E_M at which the polarization reaches the maximum is plotted in the inset also as a function of d. We observe that the height of the polarization peak increases with d and its position meanwhile shifts towards
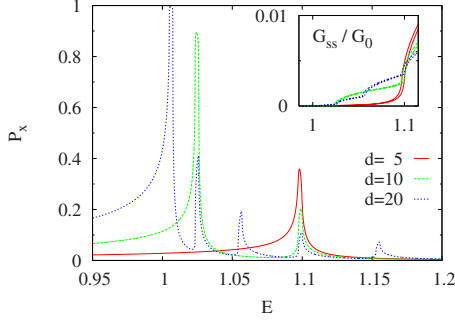
FIG. 5. (Color online) Plot of the x component of the polarization vector, P_x, and, in the inset, the spin-resolved conductances $G_{\uparrow\uparrow}$ and $G_{\downarrow\downarrow}$ as functions of energy E, for a structure consisting of two δ barriers with opposite signs of the magnetic field at distance d =5 (solid red line), 10 (long-dashed green line), 20 (short-dashed blue line), in units of ℓ_B. The Zeeman couplings are λ_x=−0.0025 and λ_z=0.005. We take B=1 T and W=$2\ell_B\approx50$ nm, and the energy is measured in units of $E_m\approx25$ meV.

lower energy. From the numerical curves we can extract the following behavior for $|P(E_M)|$ and E_M:

$$|P(E_M)| \simeq \frac{d^\alpha}{C_1 + d^\alpha}, \tag{31}$$

$$E_M \simeq E_{th} + \frac{C_2}{d^\beta}, \tag{32}$$

where E_{th}=1, $C_1\simeq1090$, $C_2\simeq1.3$, $\alpha\simeq4.0$, and $\beta\simeq1.3$. In Fig. 6 the dots represent the exact numerical results while the dashed line is the fitting curve. Upon increasing d, E_M approaches the transmission threshold relative to the first barrier. From our numerical results we also observe that C_1 grows by decreasing $|\lambda_x|$ approximately as $C_1\propto|\lambda_x|^{-1}$, while the other parameters in Eqs. (31) and (32) only weakly depend on the Zeeman couplings. For small values of $|\lambda_x|$ we do not have an efficient spin filter since the polarization peak occurs in a very narrow range of energy where $G_{\uparrow\uparrow}$ and $G_{\downarrow\downarrow}$ are both very small.

In the presence of an exchange field, instead, the effective Zeeman interaction also includes the exchange contribution
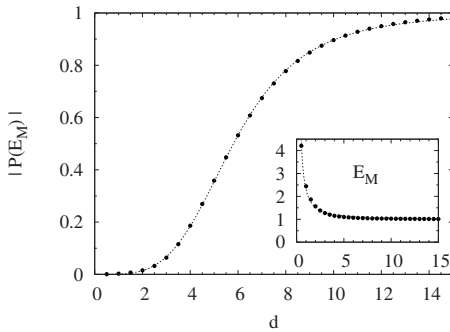
and it is thus much larger, $\lambda_x\simeq-0.2$. In this case the energy range where we get polarization effects is widened and in the spin-resolved conductance plot, Fig. 7, we can now clearly distinguish $G_{\uparrow\uparrow}$ from $G_{\downarrow\downarrow}$. In particular, within a range of approximately 10 meV we can have transmission of particles with spin up and almost perfect reflection of particles with spin down, realizing a very efficient spin filter. Indeed, in Fig. 8 we can see that, with a ferromagnetic region of width $d\sim20\ell_B\sim500$ nm, particles of energy $\Phi/2+\lambda_x\lesssim E\lesssim\Phi/2$ $-\lambda_x$ (we set λ_x negative), i.e., between approximately 20 and 30 meV, get perfectly spin filtered upon crossing the magnetic structure. The polarization, whose largest component is P_x, reaches value one and it is sizable even for a larger range of energy. The other two components of the polarization vector, P_y and P_z, due to the spin-flip processes at the barriers and shown in the insets of Fig. 8, remain very small, since λ_z is small and confined to very narrow regions under the two thin barriers.
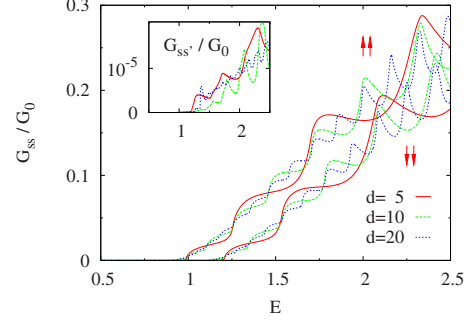

FIG. 7. (Color online) Plot of the spin-resolved conductances $G_{\uparrow\uparrow}$ and $G_{\downarrow\downarrow}$ as functions of energy (in units of $E_m\approx25$ meV) for the same structure as in Fig. 5. Here the Zeeman couplings are λ_x =−0.2 (which effectively includes the exchange contribution) and λ_z=0.005. Same line styles both for spin up and spin down. In the inset the plot of $G_{\uparrow\downarrow}=G_{\downarrow\uparrow}$ for the same parameters.

III. BILAYER GRAPHENE

In this section we consider the spin-transport problem through magnetic structures in bilayer graphene. In contrast to single-layer graphene, the low-energy dynamics of charge
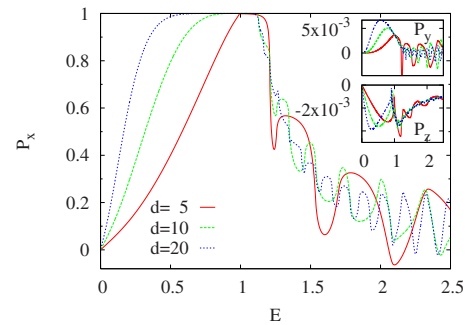

FIG. 6. Maximum of the total polarization $|P(E_M)|$ as a function of d for the same structure and parameters as in Fig. 5. In the inset: plot of the energy E_M where the peak of $|P(E)|$ is located as a function of d.

FIG. 8. (Color online) Plot of the three components of the polarization vector, P_x in the main figure, P_y and P_z in the insets, as functions of energy E (in units of $E_m\approx25$ meV) for the same structure and parameters as in Fig. 7.

carriers in bilayer graphene is governed by a quadratic Hamiltonian.[48–50] Yet, there are important differences with respect to a standard 2DEG, since the bilayer Hamiltonian has a gapless spectrum and describes *chiral* quasiparticles, i.e., the quasiparticle wave functions for fixed spin projection are two-component spinors. The effective low-energy Hamiltonian for spinful bilayer graphene reads[32,48,49]

$$H = \frac{1}{2m} \begin{pmatrix} 0 & (\pi_x - i\pi_y)^2 \\ (\pi_x + i\pi_y)^2 & 0 \end{pmatrix} + H_{spin}, \quad (33)$$

with effective mass $m \approx 0.054 m_e$ (m_e is the electron mass in vacuum) and $\pi_{x,y} = p_{x,y} + \frac{e}{c}A_{x,y}$, and H_{spin} was defined in Eq. (8). The possibility of inducing an exchange coupling by proximity of a ferromagnetic insulator has also been discussed in bilayer graphene.[32] Interestingly, in this case the electronic band structure can be drastically modified and a gap may open. However, in the simplest situation, namely, the bilayer sandwiched between two ferromagnetic insulators with the same orientation of the magnetization, the only effect is a spin splitting and Eq. (33) with a large in-plane Zeeman coupling is indeed the correct Hamiltonian.[32] Again, using $\Psi = e^{ik_y y}\psi$ the problem is reduced to a one-dimensional Schrödinger equation for a four-component wave function ψ. As in the previous section, all quantities are rescaled to be dimensionless, the only difference being that the energy scale $E_m = \hbar v_F / \ell_B$ is now replaced by $E_b = \hbar^2/2m\ell_B^2$ ($E_b \approx 1$ meV for $B=1$ T). Here we directly focus on the most interesting case of a double resonant barrier configuration in the limit of δ barriers of equal and opposite strength $\Phi = BW$, with in-plane spin splitting between the barriers. Several different magnetic field profiles have also been studied in Ref. 22 but only for the spinless case. With spin-quantization axis along the x direction, away from the δ barriers the elementary solutions of the Schrödinger equation for spin projection σ read

$$U_{\sigma\pm}(x) = \begin{pmatrix} 1 \\ \dfrac{[\pm k_{x\sigma} + i(k_y + A)]^2}{E - \sigma\lambda_x h_{ex,x}} \end{pmatrix} e^{\pm ik_{x\sigma}x}, \quad (34)$$

$$V_{\sigma\pm}(x) = \begin{pmatrix} 1 \\ \dfrac{-[\pm q_{x\sigma} - (k_y + A)]^2}{E - \sigma\lambda_x h_{ex,x}} \end{pmatrix} e^{\pm q_{x\sigma}x}, \quad (35)$$

where

$$k_{x\sigma} = \sqrt{(E - \sigma\lambda_x) - (k_y + A)^2}, \quad (36)$$

$$q_{x\sigma} = \sqrt{(E - \sigma\lambda_x) + (k_y + A)^2}, \quad (37)$$

with $\lambda_x = \mu_B B_x / E_b$ ($\lambda_x \approx -0.054$ for $B_x = -1$ T) and $\lambda_z = \mu_B BW / E_b \ell_B$. It is convenient to arrange the wave function $\psi = \psi_\uparrow |\uparrow\rangle + \psi_\downarrow |\downarrow\rangle$ and its derivative ψ' in a eight-component vector and to write it as

$$(\psi_\uparrow, \psi'_\uparrow, \psi_\downarrow, \psi'_\downarrow)^T = \mathcal{W}(x)\mathcal{A}, \quad (38)$$

where the 8×8 matrix $\mathcal{W}(x)$ is given by

$$\mathcal{W}(x) = \begin{pmatrix} U_{\uparrow+} & U_{\uparrow-} & V_{\uparrow+} & V_{\uparrow-} & 0 & 0 & 0 & 0 \\ U'_{\uparrow+} & U'_{\uparrow-} & V'_{\uparrow+} & V'_{\uparrow-} & 0 & 0 & 0 & 0 \\ 0 & 0 & 0 & 0 & U_{\downarrow+} & U_{\downarrow-} & V_{\downarrow+} & V_{\downarrow-} \\ 0 & 0 & 0 & 0 & U'_{\downarrow+} & U'_{\downarrow-} & V'_{\downarrow+} & V'_{\downarrow-} \end{pmatrix},$$

and $\mathcal{A}$ is an eight-component vector of complex amplitudes. The matching conditions at the positions $x=0, d$ of the δ barriers (i.e., continuity of the wave function and jump of its derivative) can compactly be written as

$$(\psi_\uparrow, \psi'_\uparrow, \psi_\downarrow, \psi'_\downarrow)^T(0^-) = \Omega(+)(\psi_\uparrow, \psi'_\uparrow, \psi_\downarrow, \psi'_\downarrow)^T(0^+),$$

$$(\psi_\uparrow, \psi'_\uparrow, \psi_\downarrow, \psi'_\downarrow)^T(d^-) = \Omega(-)(\psi_\uparrow, \psi'_\uparrow, \psi_\downarrow, \psi'_\downarrow)^T(d^+),$$

where the matrix Ω, nondiagonal in spin space, is given by

$$\Omega(\pm) = \begin{pmatrix} \tau_0 & 0 & 0 & 0 \\ \mp W\tau_z & \tau_0 & \mp \lambda_z \tau_x & 0 \\ 0 & 0 & \tau_0 & 0 \\ \mp \lambda_z \tau_x & 0 & \mp W\tau_z & \tau_0 \end{pmatrix}. \quad (39)$$

Finally, the transfer matrix obtains as

$$\hat{T} = \mathcal{W}(0^-)^{-1}\Omega(+)\mathcal{W}(0^+)\mathcal{W}(d^-)^{-1}\Omega(-)\mathcal{W}(d^+).$$

The scattering state for a quasiparticle of energy $E > k_y^2$ and spin projection σ incident on the structure from the left can then be written as $\mathcal{W}(x)L_\sigma$ for $x<0$ and $\mathcal{W}(x)R_\sigma$ for $x>d$, where

$$L_\sigma^T = (\delta_{\uparrow,\sigma}, r_{\uparrow\sigma}, a_\sigma, 0, \delta_{\downarrow,\sigma}, r_{\downarrow\sigma}, a'_\sigma, 0), \quad (40)$$

$$R_\sigma^T = (t_{\uparrow\sigma}, 0, 0, b_\sigma, t_{\downarrow\sigma}, 0, 0, b'_\sigma). \quad (41)$$

The transmission amplitudes $t_{\sigma\sigma'}$ are found by solving the two linear systems

$$L_\sigma = \hat{T}R_\sigma, \quad (42)$$

for $\sigma = \uparrow, \downarrow$. (This can also be easily generalized to the case of unequal strengths of the δ barriers.) Then, from Eqs. (2)–(6) we can calculate the spin-resolved conductance and the polarization.

In Fig. 9 all three components of the polarization vector are shown for two different values of d. Looking at the structure of the polarization, we can distinguish two different behaviors at two energy scales. The first occurs close to $E \sim \lambda_z \simeq 0.1$ and is dominated by spin-flip processes, as one can recognize by looking at the profile of the three components of the polarization which all exhibit some features. Indeed, at this energy scale, λ_z is not negligible and spin flips may play a role. At that energy, however, the conductance is almost zero, see Fig. 10, so spin flips can hardly be detected by direct transport measurements, at least for this value of λ_z. The second behavior occurs close to $E \sim E_{th} = \Phi/2 = 1$ which is the signature of a real spin-filter effect, as one can see from the spin-resolved conductances plotted in Fig. 10. At this energy scale λ_z is negligible and, in fact, P_y and P_z, as well as $G_{\uparrow\downarrow}$ and $G_{\downarrow\uparrow}$, which are due to spin-flip processes, practically vanish, while P_x reaches its maximum.
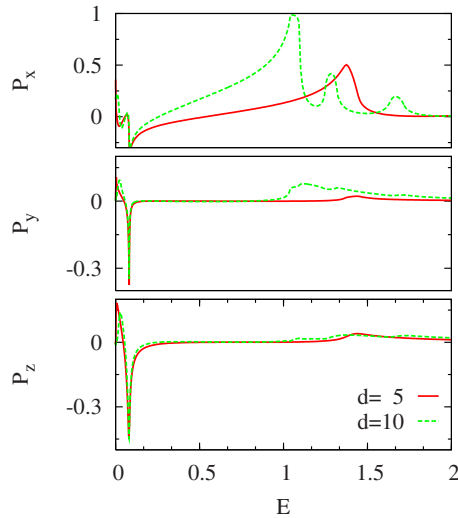
FIG. 9. (Color online) Plot of the polarization vector components in bilayer graphene for a structure consisting of two δ barriers with opposite signs of the magnetic field, $W=2$, at distance $d=5$ (solid red line) and 10 (long-dashed green line), in units of ℓ_B. The dimensionless Zeeman couplings are $\lambda_x=-0.054$ and $\lambda_z=0.108$. The energy is given in units of $E_b \approx 1$ meV, for $B=1$ T.

In the presence of a larger effective in-plane Zeeman coupling λ_x the spin-filter effect is more pronounced. In Fig. 11 the polarization vector is shown for two different values of d, with dimensionless Zeeman couplings $\lambda_x=-2$ and $\lambda_z \approx 0.1$. With this larger value of $|\lambda_x|$ the energy range in which the spin filtering occurs is significantly widened. This is also seen in the behavior of the spin-resolved conductances in Fig. 12, which shows indeed that particles with spin down are almost perfectly reflected by the magnetic structure for energies smaller than approximately 2–3 meV, while spin-up particles are almost always transmitted with spin up, since the amplitude for spin flips is very small, as shown in the inset of Fig. 12.

IV. CONCLUSIONS

In conclusion, we have analyzed the spin-transport problem through magnetic nanostructures in graphene. We have

FIG. 11. (Color online) Plot of the polarization vector components in bilayer graphene as function of energy for a structure consisting of two δ barriers with opposite signs of the magnetic field, $W=2$, at distance $d=5$ (solid red line) and 7 (long-dashed green line) (in units of ℓ_B). The dimensionless Zeeman couplings are $\lambda_x=-2$ and $\lambda_z=0.108$. The energy is given in units of $E_b \approx 1$ meV for $B=1$ T.

shown that an inhomogeneous field profile together with a strong in-plane spin splitting can produce a remarkable wave-vector-dependent spin-filtering effect. This effect is enhanced in a resonant barrier configuration, where the polarization can reach values up to one. This result can be understood by means of a simple kinematical analysis of the problem.

While we confined ourselves to zero temperature, we expect that the effect should be observable at finite temperature as well, as long as the temperature is smaller than the in-plane spin splitting. If the splitting originates from the exchange coupling and the estimate of Ref. 30 is experimentally confirmed, then there is a comfortable temperature window (say below 10 K) where the effect we discussed could, in principle, be observed. Other mechanisms inducing local ferromagnetic correlations in graphene could also be exploited to increase the spin splitting, thereby improving the
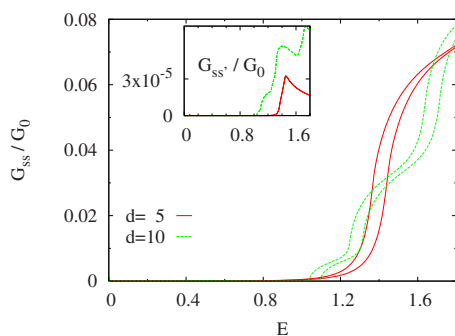

FIG. 10. (Color online) Plot of the spin-resolved conductances $G_{\uparrow\uparrow}$ and $G_{\downarrow\downarrow}$ as functions of energy (in units of $E_b \approx 1$ meV) in bilayer graphene for the same structure and parameters as in Fig. 9. Same line styles both for spin up and spin down. In the inset the plot of $G_{\uparrow\downarrow}=G_{\downarrow\uparrow}$ for the same parameters.
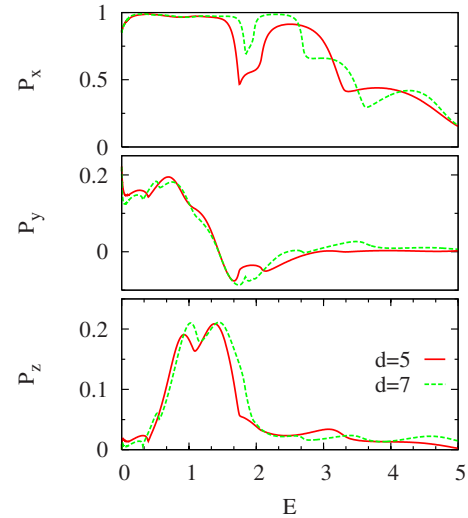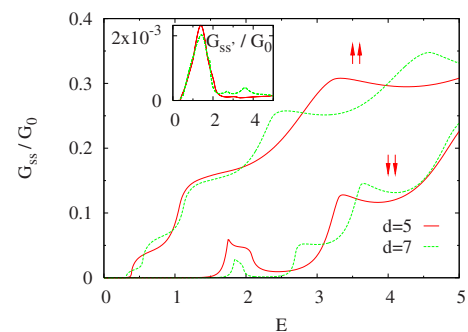

FIG. 12. (Color online) Plot of the spin-resolved conductances $G_{\uparrow\uparrow}$ and $G_{\downarrow\downarrow}$ as functions of energy (in units of $E_b \approx 1$ meV) in bilayer graphene, for the same structure and parameters as in Fig. 11. Same line styles both for spin up and spin down. In the inset the plot of $G_{\uparrow\downarrow}=G_{\downarrow\uparrow}$ for the same parameters.

spin-filtering effect. Moreover, since the orbital dynamics and the spin dynamics in this problem are to a large extent decoupled, we expect that the addition of a small amount of impurity scattering would not spoil the spin-filtering effect, at least as long as the scatterers are enough long range that they do not induce scattering between the two K points.

Along the same lines of this work, one could also investigate the effects of SOC. While the SOC has so far been estimated to be very small in graphene,[5–7] recent experimental results[51] indicate that in quasi-free-standing graphene produced on Ni(111) with intercalation of Au the Rashba effect leads to a large spin splitting on the order of 13 meV. We plan to address this problem in a forthcoming work.

Finally, we hope that our paper will stimulate further experimental research on the physics and the transport properties of magnetic nanostructures in graphene.

[1] K. S. Novoselov, A. K. Geim, S. V. Morozov, D. Jiang, Y. Zhang, S. V. Dubonos, I. V. Griegorieva, and A. A. Firsov, Science **306**, 666 (2004); Nature (London) **438**, 197 (2005).

[2] Y. Zhang, Y. W. Tan, H. L. Stormer, and P. Kim, Nature (London) **438**, 201 (2005).

[3] For recent reviews, see A. K. Geim and K. S. Novoselov, Nature Mater. **6**, 183 (2007); A. H. Castro Neto, F. Guinea, N. M. R. Peres, K. S. Novoselov, and A. K. Geim, Rev. Mod. Phys. **81**, 109 (2009).

[4] I. Žutić, J. Fabian, and S. Das Sarma, Rev. Mod. Phys. **76**, 323 (2004).

[5] D. Huertas-Hernando, F. Guinea, and A. Brataas, Phys. Rev. B **74**, 155426 (2006).

[6] Hongki Min, J. E. Hill, N. A. Sinitsyn, B. R. Sahu, L. Kleinman, and A. H. MacDonald, Phys. Rev. B **74**, 165310 (2006).

[7] Y. Yao, F. Ye, X. L. Qi, S. C. Zhang, and Z. Fang, Phys. Rev. B **75**, 041401(R) (2007).

[8] B. Trauzettel, D. V. Bulaev, D. Loss, and G. Burkard, Nat. Phys. **3**, 192 (2007).

[9] N. Tombros, C. Jozsa, M. Popinciuc, H. T. Jonkman, and B. J. van Wees, Nature (London) **448**, 571 (2007).

[10] E. W. Hill, A. K. Geim, K. S. Novoselov, F. Schedin, and P. Blake, IEEE Trans. Magn. **42**, 2694 (2006).

[11] S. Cho, Y. F. Chen, and M. S. Fuhrer, Appl. Phys. Lett. **91**, 123105 (2007).

[12] M. Nishioka and A. M. Goldman, Appl. Phys. Lett. **90**, 252505 (2007).

[13] A. De Martino, L. Dell'Anna, and R. Egger, Phys. Rev. Lett. **98**, 066802 (2007); Solid State Commun. **144**, 547 (2007).

[14] S. Park and H. S. Sim, Phys. Rev. B **77**, 075433 (2008).

[15] L. Oroszlany, P. Rakyta, A. Kormanyos, C. J. Lambert, and J. Cserti, Phys. Rev. **77**, 081403(R) (2008).

[16] T. K. Ghosh, A. De Martino, W. Häusler, L. Dell'Anna, and R. Egger, Phys. Rev. B **77**, 081404(R) (2008).

[17] W. Häusler, A. De Martino, T. K. Ghosh, and R. Egger, Phys. Rev. B **78**, 165402 (2008).

[18] F. Zhai and K. Chang, Phys. Rev. B **77**, 113409 (2008).

[19] M. Tahir and K. Sabeeh, Phys. Rev. B **77**, 195421 (2008).

[20] M. Ramezani Masir, P. Vasilopoulos, and F. M. Peeters, Appl. Phys. Lett. **93**, 242103 (2008).

[21] M. Ramezani Masir, P. Vasilopoulos, A. Matulis, and F. M. Peeters, Phys. Rev. B **77**, 235443 (2008).

[22] M. Ramezani Masir, P. Vasilopoulos, and F. M. Peeters, Phys. Rev. B **79**, 035409 (2009).

[23] Hengyi Xu, T. Heinzel, M. Evaldsson, and I. V. Zozoulenko, Phys. Rev. B **77**, 245401 (2008).

[24] A. Kormányos, P. Rakyta, L. Oroszlány, and J. Cserti, Phys. Rev. B **78**, 045430 (2008).

[25] L. Dell'Anna and A. De Martino, Phys. Rev. B **79**, 045420 (2009); **80**, 089901(E) (2009).

[26] S. Ghosh and M. Sharma, J. Phys.: Condens. Matter **21**, 292204 (2009); M. Sarma and S. Ghosh, arXiv:0907.1631 (unpublished).

[27] I. Snyman, Phys. Rev. B **80**, 054303 (2009).

[28] L. Z. Tan, C.-H. Park, and S. G. Louie, arXiv:0906.4975 (unpublished).

[29] M. Ramezani Masir, P. Vasilopoulos, and F. M. Peeters, arXiv:0907.3871, New J. Phys. (to be published).

[30] H. Haugen, D. Huertas-Hernando, and A. Brataas, Phys. Rev. B **77**, 115406 (2008).

[31] Y. G. Semenov, K. W. Kim, and J. M. Zavada, Appl. Phys. Lett. **91**, 153105 (2007).

[32] Y. G. Semenov, J. M. Zavada, and K. W. Kim, Phys. Rev. B **77**, 235415 (2008).

[33] N. M. R. Peres, F. Guinea, and A. H. Castro Neto, Phys. Rev. B **72**, 174406 (2005).

[34] O. V. Yazyev and L. Helm, Phys. Rev. B **75**, 125408 (2007).

[35] Y.-W. Son, M. L. Cohen, and S. G. Louie, Nature (London) **444**, 347 (2006).

[36] T. Yokoyama, Phys. Rev. B **77**, 073413 (2008).

[37] Z. P. Niu, F. X. Li, B. G. Wang, L. Sheng, and D. Y. Xing, Eur. Phys. J. B **66**, 245 (2008).

[38] V. Nam Do, V. Hung Nguyen, P. Dollfus, and A. Bournel, J. Appl. Phys. **104**, 063708 (2008).

[39] Y.-X. Li, Eur. Phys. J. B **68**, 119 (2009).

[40] See, for example, I. S. Ibrahim and F. M. Peeters, Phys. Rev. B **52**, 17321 (1995).

[41] F. Zhai and H. Q. Xu, Phys. Rev. Lett. **94**, 246601 (2005).

[42] F. Zhai and H. Q. Xu, Appl. Phys. Lett. **88**, 032502 (2006).

[43] B. K. Nikolic and S. Souma, Phys. Rev. B **71**, 195328 (2005).

[44] M. Scheid, D. Bercioux, and K. Richter, New J. Phys. **9**, 401 (2007).

[45] I. S. Gradshteyn and I. M. Ryzhik, *Table of Integrals, Series, and Products*, 6th ed. (Academic, San Diego, 2000).

[46] G. N. Watson, Proc. London Math. Soc. **s2-8**, 393 (1910); see also N. Schwid, Trans. Am. Math. Soc. **37**, 339 (1935).

[47] B. H. J. McKellar and G. J. Stephenson, Jr., Phys. Rev. A **36**, 2566 (1987).

[48] K. S. Novoselov, E. McCann, S. V. Morozov, V. I. Fal'ko, M. I. Katsnelson, U. Zeitler, D. Jiang, F. Schedin, and A. K. Geim, Nat. Phys. **2**, 177 (2006).

[49] E. McCann and V. I. Fal'ko, Phys. Rev. Lett. **96**, 086805 (2006).

[50] M. I. Katsnelson, K. S. Novoselov, and A. K. Geim, Nat. Phys. **2**, 620 (2006).

[51] A. Varykhalov, J. Sánchez-Barriga, A. M. Shikin, C. Biswas, E. Vescovo, A. Rybkin, D. Marchenko, and O. Rader, Phys. Rev. Lett. **101**, 157601 (2008).